engineering proceedings

MDPI

Proceeding Paper

Synthesis and Characterization of Three-Dimensional Nanoporous Copper Oxide Materials via Dealloying and Thermal Oxidation of Amorphous Ribbons †

Mircea Nicolaescu [1,2], Cosmin Codrean [2], Corina Orha [1] and Cornelia Bandas [1,*]

[1] National Institute for Research and Development in Electrochemistry and Condensed Matter, A. Paunescu Podeanu Street, No 144, 300569 Timisoara, Romania; nicolaescu.mircea13@yahoo.com (M.N.); orha.corina@gmail.com (C.O.)

[2] Department of Materials and Manufacturing Engineering, Faculty of Mechanical Engineering, Politehnica University Timisoara, P-ta Victoriei, No. 2, 300006 Timisoara, Romania; cosmin.codrean@upt.ro

* Correspondence: cornelia.bandas@gmail.com

† Presented at the 2nd International Electronic Conference on Chemical Sensors and Analytical Chemistry, 16–30 September 2023; Available online: https://csac2023.sciforum.net/.

Abstract: The synthesis of nanoporous copper oxide (NP-CuO) materials via the dealloying and thermal oxidation of amorphous CuZrAl ribbons, representing the novelty of this research and previously achieved via a melt-spinning process, was carried out in an aqueous hydrofluoric acid (HF) solution by varying the holding time. These nanoporous copper (NPC) structures were used as a template to achieve a 3D-NP-CuO materials with different surface morphologies. To investigate the structural and morphological properties of the obtained sandwich-type materials, X-ray diffraction (XRD), scanning electron microscopy coupled with energy-dispersive x-ray spectroscopy (SEM/EDX), and ultraviolet–visible spectroscopy (UV-VIS) techniques were used. In summary, the dealloying and thermal oxidation of amorphous ribbons is an interesting approach to achieving a three-dimensional (3D) network of NP-CuO with different morphologies and with a low production cost. These sandwich-type structures, consisting of NPC and copper oxide nanowires (CuO/Cu_2O), combine the good electrical properties of NPC with the catalytic properties of copper oxide semiconductors, making them suitable materials for photocatalysis, photoelectrodes in solar cells, battery applications, and electrochemical sensors.

Keywords: amorphous ribbons; dealloying; thermal oxidation; nanoporous copper oxide; nanowires

Citation: Nicolaescu, M.; Codrean, C.; Orha, C.; Bandas, C. Synthesis and Characterization of Three-Dimensional Nanoporous Copper Oxide Materials via Dealloying and Thermal Oxidation of Amorphous Ribbons. *Eng. Proc.* **2023**, *48*, 56. https://doi.org/10.3390/CSAC2023-15171

Academic Editor: Nicole Jaffrezic-Renault

Published: 20 October 2023

1. Introduction

Metal oxide semiconductors are very attractive materials for several industries, particularly for the energy conversion sector, sensor industry, and environment remediation industry [1–3]. Copper has two oxidation state oxides, cupric oxide (CuO) and cuprous oxide (Cu_2O), which both have semiconductor properties with band gaps of 1.2 and 2.0 eV, respectively. Their energy band gaps make them good candidates for solar cells, water-splitting devices, and sensor devices [1,4]. Nanoporous materials are an important class of functional material that can improve material properties because of their large surface area and surface-to-weight ratio [5]. The dealloying process is one of the routes to producing nanoporous and microporous materials via the selective dissolution of less noble elements in acidic or basic solution [6,7]. Amorphous ribbons have a homogeneous composition and, compared to crystalline alloys, do not have grain boundaries or defects, making them an ideal candidate for the dealloying process [8]. Through the dealloying process using amorphous materials, nanoporous gold (NPG) [9], nanoporous silver (NPS) [10], nanoporous platinum (NPP) [11], nanoporous nickel (NPN) [12], and nanoporous copper (NPC) [13] were synthesized, as well as other nanoporous composite materials (metal–metal or metal-oxide) [14,15].

The synthesis of NPCs via dealloying has been studied by groups of researchers around the world in bulk or ribbon form, from various amorphous alloy systems. Dan et al. [14], produce an NPC structure from TixCu100x amorphous binary alloys (x = 40, 50 and 60%) in hydrofluoric acid solution under free corrosion conditions. The tapes that were dealloyed in HF solution with a concentration of 0.03 M showed a bicontinuous nanoporous structure with a pore size of 25 to 75 nm and a ligament size of 46 to 79 nm. The dealloyed ribbons in 0.13 M HF solution had a pore size of 85–380 nm and a ligament size of 80–338 nm [8].

Li et al. [15] presented a relatively simple two-step synthesis method (dealloying–electrochemical oxidation) to produce Cu_2O/CuO nanoporous oxide heterostructures using massive amorphous metal rods (BMG). The NPC was manufactured by chemically dealloying the bulk alloy rod $Cu_{50}Zr_{45}Al_5$ (BMG) in 0.05 M HF at 298 K for 1 day. The growth of CuO and Cu_2O heterostructures was carried out electrochemically at a temperature of 298 K in 0.5 M KOH and at a constant current density of 5 mA cm^{-2} for 10–30 min [15].

Thermal oxidation is one of the simplest processes for producing a wide range of micro- and nano-oxide structures, such as nanowires, nanoflakes, and nanoneedles, on a metal surface [16–18]. This process involves heating metal substrates, such as foil, plates, and wires, in the presence of air. Amorphous ribbons from CuZr systems have been widely used as dealloying alloys and as nanostructured oxides for various applications. Their Zr and Al standard equilibrium potentials are larger than those for Cu [4,19]. The difference in the standard electrode potentials between these elements means that the Cu–Zr-Al amorphous alloy meets the requirements for dealloying.

In the present work, an NPC substrate produced via the free dealloying process of CuZrAl ribbons was used as a template to obtain nanoporous copper oxide via the thermal oxidation process. The influence of holding time at a temperature of 500 °C on the surface morphology was also discussed.

2. Materials and Methods

2.1. Preparation of Amorphous Ribbons

To produce an amorphizable alloy with the nominal composition of $Cu_{48}Zr_{47}Al_5$, the arc melting process was used with a mixture of pure Cu (99.99 wt%), pure Zr (99.9 wt%), and Al (99.9 wt%) in an Ar atmosphere. A CuZrAl amorphous ribbon was prepared using the melt-spinning method. As-produced ribbons had a thickness of 20 µm and a width of 2 mm. The dealloying process was carried out in a 0.5 M HF solution, purchased from the Sigma-Aldrich Company (St. Louis, MO, USA), under free immersion at room temperature for a reaction time of 2 h. After corrosion, the ribbons were washed with distilled water to remove any residual HF solution.

2.2. Thermal Oxidation Process

Thermal oxidation of the prepared nanoporous ribbons was carried out at 500 °C for 6, 12, and 24 h in air atmosphere. The heating rate (10 °C/min) was maintained until the oxidation temperatures were reached.

2.3. D-NP-CuO Material Characterization

To study the structure of the Cu-Zr-Al ribbons before and after dealloying, and also after thermal oxidation, X-ray diffraction (XRD) patterns were collected using a PANalytical X'Pert PRO MPD diffractometer with Cu-Kα radiation (λ = 1.5418 Å), in the range of 2θ = 10–80°, from Almelo, the Netherlands. The surface morphology of the samples obtained before and after thermal oxidation was examined via scanning electron microscopy (SEM) using an Inspect S + EDAX GENESIS XM 2i microscope from the FEI Company from Eindhoven, the Netherlands. Energy-dispersive X-ray spectroscopy was conducted for elemental identification of the samples using an EDX Ametek Element Module from Eindhoven, the Netherlands. The optical properties of the material were recorded using a UV-Vis analysis PerkinElmer Lambda 950 UV/Vis spectrophotometer, in the range of

350–800 nm, from Connecticut, USA. The band gap Eg of the materials was determined by plotting the Kubelka–Munk function against energy (eV).

3. Results and Discussion

The XRD patterns of the amorphous and dealloyed ribbons are illustrated in Figure 1a. A broad intensity peak appears in the XRD diffraction patterns of the amorphous ribbons at an angle of 2θ in the range of 35–45°, which reflects the amorphous state of the CuZrAl alloy. After the dealloying process, the most electrochemically active elements (Zr and Al) were selectively removed. The nonporous metal is mainly composed of face-centered cubic (fcc) Cu (JCPDS card No. 00-004-0836) and some cubic Cu_2O (JCPDS card No. 01-078-2076). The Cu_2O nanoparticle was obtained on the NPC substrate, probably because the dealloying method was carried out in an oxygen-rich corrosive solution, resulting in some of the copper atoms of the NPC reacting with the dissolved oxygen, resulting in Cu_2O nanoparticles [20]. Figure 1b shows the XRD patterns of the as-synthesized 3D-NP-CuO material, after thermal oxidation. Due to the high surface area of the NPC ribbons after thermal oxidation, copper atoms react with the oxygen in the atmosphere and the sample becomes primarily composed of monoclinic CuO (JCPDS card No. 00-005-0661) for all thermal oxidation parameters. Based on XRD results and according to the literature data, it can be concluded that the formation process of the produced CuO nanoparticles and nanowires includes two reaction steps [21]:

$$4Cu + O_2 \rightarrow Cu_2O; \quad (1)$$

$$2Cu_2O + O_2 \rightarrow CuO; \quad (2)$$

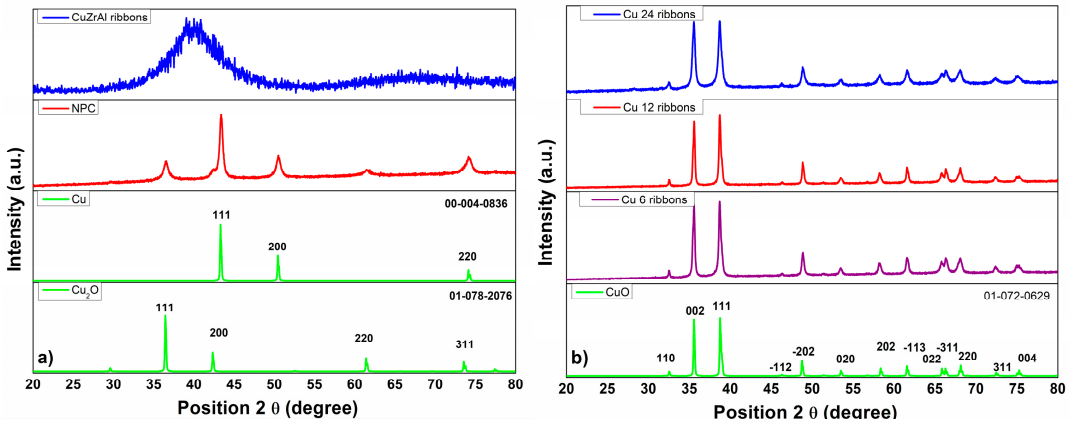

Figure 1. XRD pattern of copper base amorphous ribbons for (**a**) amorphous and nanoporous cooper and (**b**) 3D-NP-CuO material.

Figure 2 shows the surface morphology of the as-dealloyed CuZrAl amorphous ribbons in a 0.5 M HF solution at room temperature during a 2 h holding time. The pore size was measured from SEM images using ImageJ software (Version 1.53t) and defined as the distance between the ligaments/particles. The dealloyed $Cu_{48}Zr_{47}Al_5$ amorphous ribbon presents a 3D bicontinuous nonporous structure with an average ligament length of 26.75 nm. This structure resulted from the rearrangement of the copper atom after zirconium and aluminum were removed. The Cu_2O structure shown in the XRD pattern (Figure 1a) is not clearly highlighted in the SEM image (Figure 2a), possibly due to the nanosize of the Cu_2O particles. In Figure 2b–d, samples with different surface morphologies synthesized through the thermal oxidation process are presented.

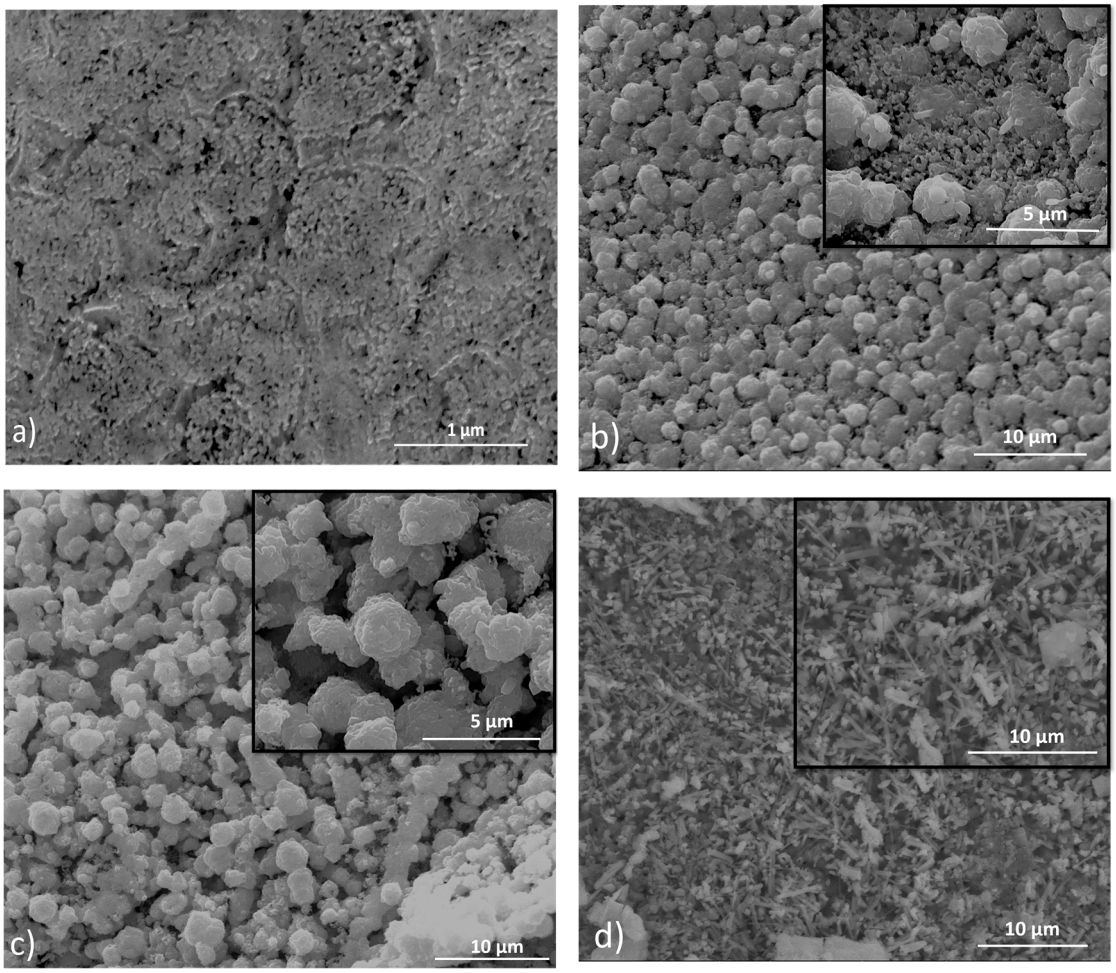

Figure 2. SEM morphologies of the NPC and NP-CuO samples for (**a**) NPC; (**b**) NP-CuO obtained at 500 °C with a holding time of 6 h; (**c**) NP-CuO obtained at 500 °C with a holding time of 12 h; and (**d**) NP-CuO obtained at 500 °C with a holding time of 24 h.

Figure 2b shows SEM images of the thermal oxidation sample at 500 °C with a holding time of 6 h. It can be seen that the synthesized monoclinic CuO material presents a homogeneous distributed 3D interconnected sphere, which is composed of many nanorods. The 3D copper oxide nanoparticles show a nanopore structure mimicking the NPC template [22]. From the inset of Figure 2b, it can be seen that larger spheres are formed on a 3D substrate compound from smaller interconnected nanorods and much smaller nanospheres. The average length of the surface sphere is 1.63 µm, and the average distance between them is about 505 nm. The distance between the 3D substrates is about 152 nm. Figure 2c presents an SEM image of the sample obtained at a 12 h holding time. The 3D interconnected spheres of the CuO material have an increase in surface oxidation and porosity, and the larger spheres are, on average, 160 µm and the average distance between particles is 936 nm. In Figure 2d, due to the increase in the holding time to 24 h on the surface of the 3D CuO material, the in-situ growth of CuO nanowires continues, with an average length of 196 nm. The nanowires are randomly distributed on the 3D CuO surface, further increasing the surface-to-volume ratio.

The typical EDX spectra shown in Figure 3 confirm the complete dealloying of Zr and Al atoms from the amorphous ribbons. The effect of the diffusion of oxygen from the dealloying process and the natural oxidation of the nanoporous ribbons on the oxygen element is presented in Figure 3a. Figure 3b–d present an increase in oxygen content after thermal oxidation and the presence of a single metal element (Cu). A site increase in the O atom is shown in Figure 3d, due to the oxide nanowire on the NP-CuO surface.

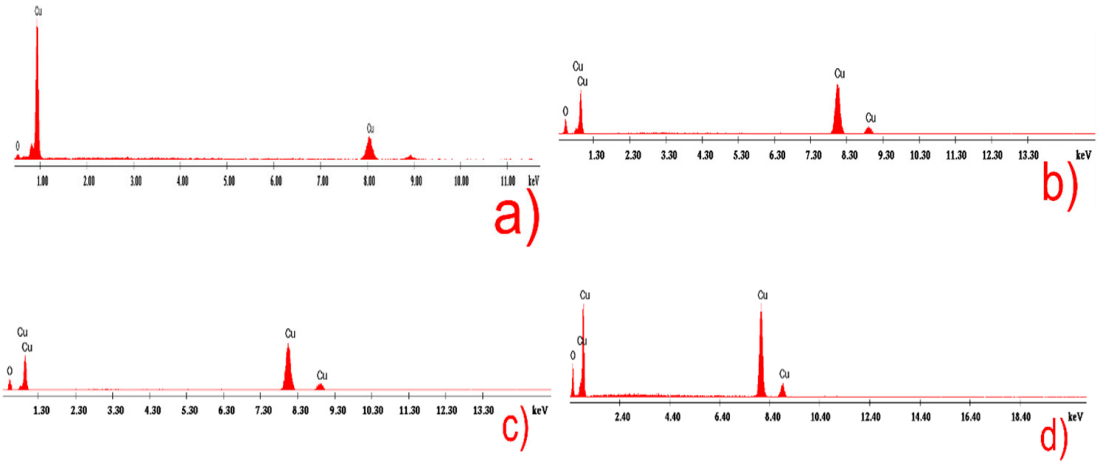

Figure 3. EDX spectrum of NPC and NP-CuO samples for (**a**) NPC; (**b**) NP-CuO obtained at 500 °C with a 6 h holding time; (**c**) NP-CuO obtained at 500 °C with a 12 h holding time; and (**d**) NP-CuO obtained at 500 °C with a 24 h holding time.

The UV-vis absorption spectra of the synthesized NP-CuO are shown in Figure 4a. The absorption spectra are present a very high absorption in both the visible region and the UV region, which is probably due to the nanoporous oxide structure [23]. The optical band gaps of the NP-CuO materials were determined using the Tauc plot method, using Equation (3) [24]:

$$\alpha hm = A(hv - Eg)^n \quad (3)$$

where α is the absorption coefficient, hv is the photon energy, A is a proportionality constant, and Eg is the optical band gap.

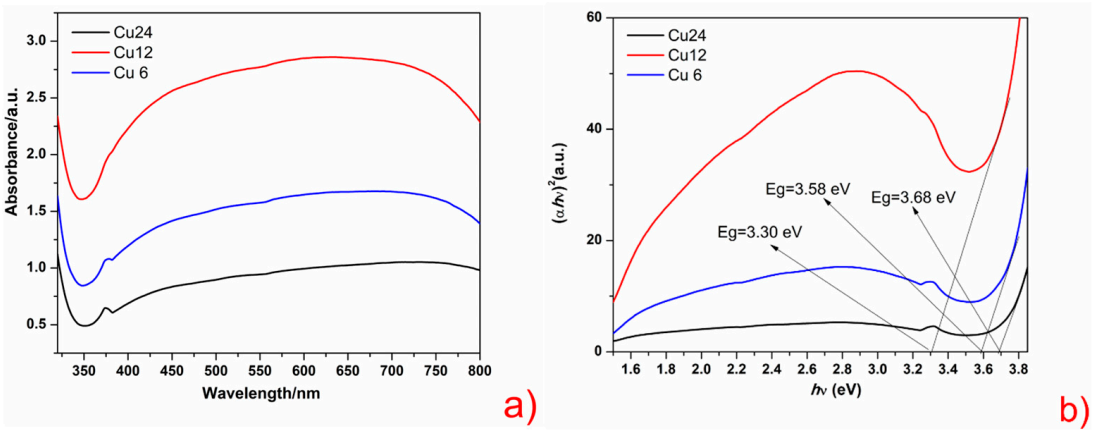

Figure 4. (**a**) Absorption spectra and (**b**) band gap values of the as-synthesized samples at different temperatures.

p-type CuO semiconductors have reported optical band gaps between 1.3 and 2.1 eV [25]. In our study, for the NP-CuO samples, a high band gap at 3.68 eV was reported for the surface nanowire sample. For the sample oxidized for 6 and 12 h, band gaps at 3.58 and 3.30 eV, respectively, were presented. A slight increase in the band for the material synthesized for 24 h was due to the unidimensional structure on the NP-CuO surface. A blue shift was indicated from our results, generated by the reduced particle size. This blue shift has been reported in the literature for CuO quantum dots, because of quantum confinement effects [26,27].

4. Conclusions

In summary, the dealloying and thermal oxidation of amorphous ribbons is an interesting approach to achieving 3D networks of NP-CuO with different morphologies and

with a low production cost. The absorption spectra of NP-CuO samples show a wide absorption band in the 350–800 nm region and a high surface-to-volume ratio, which can lead to enhanced photocatalytic activity for environmental remediation. Because of the wide absorption spectra, NP-CuO might be used as an ideal harvester for solar irradiation. At an increased holding time of 24 h, on the surface of NP-CuO, successfully unidimensional nanowires were synthesized. For the first time, in this work, a high-energy band gap value in the range of 3.30 eV to 3.68 eV was reported for CuO nanoparticles obtained via the dealloying and thermal oxidation of amorphous ribbons.

Author Contributions: M.N. was involved in the conceptualization, methodology, investigation, and writing—original draft; C.C. was involved in the conceptualization, methodology, investigation, and writing—original draft; C.O. was involved in the conceptualization, methodology, investigation, and writing—original draft; C.B. was involved in the methodology, investigation, writing—original draft, and supervision. All authors have read and agreed to the published version of the manuscript.

Funding: This work was supported by a grant from the Ministry of Research, Innovation and Digitization, CNCS-UEFISCDI, project number PN-III-P1-1.1-TE-2021-0963, within PNCDI III, with contract number TE13/2022 (DD-CyT); by the project "Network of excellence in applied research and innovation for doctoral and postdoctoral programs/InoHubDoc", co-funded by European Social Fund financing agreement no. POCU/993/6/13/153437; and partially by project code PN 23 27 01 02 INOMAT, 23-27 29N/2023.

Institutional Review Board Statement: Not applicable.

Informed Consent Statement: Not applicable.

Data Availability Statement: Not applicable.

Conflicts of Interest: The authors declare no conflict of interest.

References

1. Vajda, M.; Ursu, D.; Miclau, N.; Duteanu, N.; Miclau, M. Fabrication of copper oxide-based dye-sensitized solar cell with high short-circuit current density (JSC) using flexible and binder-free porous photoelectrode. *J. Mater. Sci. Mater. Electron.* **2022**, *33*, 20790–20801. [CrossRef]
2. Liu, D.; Yang, Z.; Wang, P.; Li, F.; Wang, D.; He, D. Preparation of 3D nanoporous copper-supported cuprous oxide for high-performance lithium ion battery anodes. *Nanoscale* **2013**, *5*, 1917–1921. [CrossRef]
3. Liu, X.; Du, J.; Shao, Y.; Zhao, S.F.; Yao, K.F. One-pot preparation of nanoporous Ag-Cu@Ag core-shell alloy with enhanced oxidative stability and robust antibacterial activity. *Sci. Rep.* **2017**, *7*, 10249. [CrossRef]
4. Zhou, M.; Huang, X.; Hagos, K.; Cui, Y.; Ma, L. Nanoporous copper fabricated from $Zr_{65}Cu_{17.5}Fe_{10}Al_{7.5}$ amorphous alloy and its electrocatalytic oxidation performance. *Intermetallics* **2017**, *90*, 23–29. [CrossRef]
5. Wang, Y.M.; Zhang, W.; Inoue, A. Nanoporous Cu wide ribbons with good mechanical integrity. *Mater. Sci. Eng. B* **2012**, *177*, 532–535. [CrossRef]
6. McCue, I.; Benn, E.; Gaskey, B.; Erlebacher, J. Dealloying and Dealloyed Materials. *Annu. Rev. Mater. Res.* **2016**, *46*, 263–286. [CrossRef]
7. An, Y.; Tian, Y.; Wei, C.; Tao, Y.; Xi, B.; Xiong, S.; Feng, J.; Qian, Y. Dealloying: An effective method for scalable fabrication of 0D, 1D, 2D, 3D materials and its application in energy storage. *Nano Today* **2021**, *37*, 101094. [CrossRef]
8. Dan, Z.; Qin, F.; Yamaura, S.-I.; Sugawara, Y.; Muto, I.; Hara, N. Dealloying behavior of amorphous binary Ti–Cu alloys in hydrofluoric acid solutions at various temperatures. *J. Alloys Compd.* **2013**, *581*, 567–572. [CrossRef]
9. Chao, B.K.; Xu, Y.; Ho, H.C.; Yiu, P.; Lai, Y.C.; Shek, C.H.; Hsueh, C.H. Gold-rich ligament nanostructure by dealloying Au-based metallic glass ribbon for surface-enhanced Raman scattering. *Sci. Rep.* **2017**, *7*, 7485. [CrossRef]
10. Jin, Y.; Li, R.; Zhang, T. Formation of nanoporous silver by dealloying Ca–Ag metallic glasses in water. *Intermetallics* **2015**, *67*, 166–170. [CrossRef]
11. Wang, S.; Li, H.; Lin, H.; Wu, K. Enhanced electro-catalytic performance of Pd-based hierarchical nanoporous structures fabricated by micropatterning and dealloying of Pd-Ni-P metallic glass. *Nanotechnology* **2020**, *31*, 155301. [CrossRef] [PubMed]
12. Zheng, D.; Zhao, F.; Li, Y.; Qin, C.; Zhu, J.; Hu, Q.; Wang, Z.; Inoue, A. Flexible NiO micro-rods/nanoporous Ni/metallic glass electrode with sandwich structure for high performance supercapacitors. *Electrochim. Acta* **2019**, *297*, 767–777. [CrossRef]
13. Wang, Z.; Liu, J.; Qin, C.; Liu, L.; Zhao, W.; Inoue, A. Fabrication and new electrochemical properties of nanoporous Cu by dealloying amorphous Cu–Hf–Al alloys. *Intermetallics* **2015**, *56*, 48–55. [CrossRef]
14. Dan, Z.; Qin, F.; Makino, A.; Sugawara, Y.; Muto, I.; Hara, N. Fabrication of nanoporous copper by dealloying of amorphous Ti–Cu–Ag alloys. *J. Alloys Compd.* **2014**, *586*, S134–S138. [CrossRef]

15. Li, M.; Li, Y.; Zhang, Q.; Qin, C.; Zhao, W.; Wang, Z.; Inoue, A. Ultrafine Cu_2O/CuO nanosheet arrays integrated with NPC/BMG composite rod for photocatalytic degradation. *Appl. Surf. Sci.* **2019**, *483*, 285–293. [CrossRef]
16. Filipic, G.; Cvelbar, U. Copper oxide nanowires: A review of growth. *Nanotechnology* **2012**, *23*, 194001. [CrossRef]
17. Li, A.; Song, H.; Wan, W.; Zhou, J.; Chen, X. Copper oxide nanowire arrays synthesized by in-situ thermal oxidation as an anode material for lithium-ion batteries. *Electrochim. Acta* **2014**, *132*, 42–48. [CrossRef]
18. Nicolaescu, M.; Orha, C.; Dabici, A.; Hididis, P.; Codrean, C.; Șerban, V.A. Production of Cu-Zr mixed metal oxides by thermal oxidation of amorphous ribbons. *Mater. Today Proc.* **2021**, *45*, 4337–4343. [CrossRef]
19. Lu, H.-B.; Li, Y.; Wang, F.-H. Synthesis of porous copper from nanocrystalline two-phase Cu–Zr film by dealloying. *Scr. Mater.* **2007**, *56*, 165–168. [CrossRef]
20. Wang, Z.; Liu, J.; Qin, C.; Yu, H.; Xia, X.; Wang, C.; Zhang, Y.; Hu, Q.; Zhao, W. Dealloying of Cu-Based Metallic Glasses in Acidic Solutions: Products and Energy Storage Applications. *Nanomaterials* **2015**, *5*, 697–721. [CrossRef]
21. Zhu, D.; Wang, L.; Yu, W.; Xie, H. Intriguingly high thermal conductivity increment for CuO nanowires contained nanofluids with low viscosity. *Sci. Rep.* **2018**, *8*, 5282. [CrossRef]
22. Sasikala, N.T.; Boominathasellarajan, S.; Raghupathy, B.P.C. Fabrication of Nanostructures Using Porous Anodic Alumina Template. *Int. J. Nanosci.* **2012**, *10*, 783–786. [CrossRef]
23. Bin Mobarak, M.; Hossain, M.S.; Chowdhury, F.; Ahmed, S. Synthesis and characterization of CuO nanoparticles utilizing waste fish scale and exploitation of XRD peak profile analysis for approximating the structural parameters. *Arab. J. Chem.* **2022**, *15*, 104117. [CrossRef]
24. Makula, P.; Pacia, M.; Macyk, W. How to Correctly Determine the Band Gap Energy of Modified Semiconductor Photocatalysts Based on UV-Vis Spectra. *J. Phys. Chem. Lett.* **2018**, *9*, 6814–6817. [CrossRef] [PubMed]
25. Murali, D.S.; Kumar, S.; Choudhary, R.J.; Wadikar, A.D.; Jain, M.K.; Subrahmanyam, A. Synthesis of Cu_2O from CuO thin films: Optical and electrical properties. *AIP Adv.* **2015**, *5*, 047143. [CrossRef]
26. Rehman, S.; Mumtaz, A.; Hasanain, S.K. Size effects on the magnetic and optical properties of CuO nanoparticles. *J. Nanoparticle Res.* **2010**, *13*, 2497–2507. [CrossRef]
27. Schmid, G. *Nanoparticles from Theory to Application*, 1st ed.; Wiley-VCH Verlag GmbH & Co.: Weinheim, Germany, 2004.